This is a peer-reviewed, accepted author manuscript of the following research article: Wei, D., Zhao, W., Wan, D., & Xiao, Q. (2021). A new method for simulating multiple wind turbine wakes under yawed conditions. *Ocean Engineering*, *239*, [109832]. https://doi.org/10.1016/j.oceaneng.2021.109832

A new method for simulating multiple wind turbine wakes under yawed conditions

Dezhi Wei[1], Weiwen Zhao[1], Decheng Wan[1]*, Qing Xiao[2]

[1]Computational Marine Hydrodynamics Lab (CMHL), School of Naval Architecture, Ocean and Civil Engineering, Shanghai Jiao Tong University, Shanghai, China
[2] Department of Naval Architecture, Ocean and Marine Engineering, University of Strathclyde, Glasgow G4 0LZ, UK

* Correspondence author: dcwan@sjtu.edu.cn; Tel.: +86-21-3420- 8437

Abstract: Counter-rotating vortices generated in wake steering not only deform the turbine wake, but also can make the wake trajectory of a non-yawed downwind turbine deviate from its rotor centerline, referred to as "secondary wake steering" phenomenon. Recent studies have also shown that the vortex interactions become clearer when the wind farm includes multiple turbines. However, in the common analytical models for active yaw control, the effects of these vortices are not considered. Evidently, this omission can lead to a decrease in model prediction accuracy. To compensate for it, a new analytical wind farm model is proposed. It adopts a physical-based momentum conserving wake superposition method to deal with the interaction of multiple wakes, in which, not only combining the streamwise velocity deficit of each individual yawed wind turbine, but also the transverse velocity from different wakes. Additionally, an "added yaw angle" is defined for a downwind turbine operating in upstream yawed turbine wakes, to reflect the change in local wind direction it perceives. For validation purposes, the LES wind field obtained from the SOWFA tool is used as a reference, and the newly proposed model is found to agree well with LES results and outperforms the representative conventional analytical model in almost all test cases. The new model can successfully reproduce the "secondary wake steering" phenomenon in the overlapped wake, and provides significant improvements in predicting power production of wind turbines.

Keywords: yawed wind turbine; secondary wake steering; momentum-conserving wake superposition method; added yaw angle

1. Introduction

Wake interaction is the main cause of power losses in wind farms, and it can lead to an increase in the fatigue loads of downwind turbines. Statistics have shown that the average annual loss caused by wakes may account for about 10% to 20% of the total power production [1]. In order to mitigate these adverse effects, researchers have developed some active wake control strategies. Some examples include [2-4], among which, the active yaw control is considered to be the most effective[5] and has received much attention. The idea behind such an operational control is to decrease the wake losses of the downstream turbines by intentionally altering the yaw angle of the controlled upwind turbine. By doing so, although the misaligned upstream wind turbine experiences an individual power loss, it can potentially increase the whole wind farm power production [6].

To apply active yaw control in real-world engineering, it is crucial to have a detailed understanding of the aerodynamic performance and wake flow behavior of yawed turbines. Focusing on a single horizontal axis wind turbine, Campo et al. [7] compared the difference of the aerodynamic loads exerted on the blade in yawed flow and axis flow. To systematically investigate the main turbine characteristics, Bastankhah and Porte-agle [8] performed several experiments on a three-blade wind turbine in a neutrally stratified boundary layer. The results indicated that, both power production and thrust force of the wind turbine decrease with increasing yaw angle, and a

larger thrust coefficient was seen in the higher tip speed ratio. This is in agreement with other published researches [9,10]. In Lee et al.[11], they found that the yaw of wind turbine can not only affect the development of a skewed wake structure, but also cause the cyclic variation in induced velocity and aerodynamic load. What's more, van Dijk et al. [12] experimentally studied the effects of yaw on power production and loads for full and partial wake overlap. In their studies, an increase in the combined power production of the wind farm was seen when the upstream turbine yaws, and the loads on the downstream turbine was reduced in partial wake overlap. Similar conclusions were also drawn by Bartl et al [13]. More information on turbine thrust and power variation with the yaw angle can be found in Ref. [14-16]. Additionally, by using large-eddy simulation, Jiménez et al. [17] made an attempt to study the characteristics of wake deflection under different operating conditions, and observed that it increases with yaw angle and thrust coefficient. Bartl et al. [18] investigated the effect of inflow turbulence and shear on wake features behind a yawed turbine. In a LES study by Vollmer et al.[19], the variation of wake shape and deflection magnitude with atmospheric stability was discussed. Under uniform flow, Howland et al. [20] conducted a wind tunnel test on a porous disk turbine with yaw angles. They used different method to quantify the wake center deflection, and studied the formation of curled wake morphology, and attributed it to a pair of counter-rotating vortices (hereafter CPV) that shed from the rotor plane. Later, in Bastankhah et al. [21], the potential flow theory was applied to further analyze the mechanism of the "CPV". Apart from deforming the wake, the impact of the counter-rotating vortices was seen to become clearer when the wind farm includes multiple turbines [22,23]. The most important is that since the presence of these vortices, an upstream yawed wake can deflect the wake of a downstream turbine, even if it is non-yawed. This is called "secondary wake steering" phenomenon. The yawed wake combinations are also shown to involve merging of generated cross flows, indicating that it is necessary to include the vortex interactions for developing more effective wind farm controllers based on active yaw control. Moreover, there are also some studies that focus on the possibilities of power optimization through active yaw control. For example, in wind tunnel experiments, Bastankhah et al. [24] studied the performance of a model wind farm with five turbine rows at various yaw angle distributions. They found that the maximum total power enhancement can reach 17% for the tested wind farm, and affected by the aforementioned vortex interactions, the optimal yaw angle distribution roughly follows a linear relationship from front to rear turbine. A computational study by Gebraad et al. [25] on six wind turbines also demonstrated the capability of active yaw control, in which, a 13% increase of the combined power under yawed conditions was seen compared to the reference case with all turbines aligned.

Besides high fidelity but costly numerical simulations and wind tunnel measurements, researchers have also developed some analytical models for yawed wind turbine wakes. Due to the advantages of simplicity and high efficiency, these models are widely used in engineering scenarios requiring fast predictions. The first yawed wake model was proposed by Jimenez et al. [17], assuming top-hat distributions of the streamwise velocity deficit and the skew angle. It is commonly used with the wake recovery model of Jensen [26]. Despite its widely applications, the Jiménez model was found to be inaccurate because the top-hat wake velocity deficit is not realistic [27]. In fact, the lateral profile of normalized velocity deficit in the turbine wake approximately follows a self-similar Gaussian distribution, which has been reported in many previous researches[28,29]. As such, several Gaussian-based two dimensional (2D) analytical models were developed. One of the typical is derived by Bastankhah et al. [21]. However, although its predictions show good agreement with the experimental data, some of the model parameters are difficult to find universal values, their current estimates greatly rely on numerical simulations or experiments. Consequently, the application of the Bastankhah model is greatly restricted. The model of Dou et al.[30] also faces a similar dilemma. Later, Qian et al. [31] developed a different Gaussian model for predicting wake velocity in the far-wake region. In it, the input parameters are determined by ambient turbulence intensity and thrust coefficient, which enhances the model applicability. But studies [27] shown that the Qian model tends to underestimate the wake velocity deficit, especially for cases with small yaw angles. Adopting the same assumptions as the Qian model, Wei and Wan [32] also derived an analytical model for yawed

turbine wakes, by incorporating the yaw effects into a classical Gaussian-based non-yawed wake model. What's more, according to a relationship between the wake velocity components and the skew angle, the Wei-Wan model is extended to incorporate the prediction on the transverse velocity, which distinguish it from other common analytical models. More importantly, the model is simple in form, only the wake width growth rate is required to be specified. More details about the Wei-Wan model are given in Section 2.1 below.

Although some of these 2D models can accurately predict the wake behind a single yawed turbine, their ability in modeling larger arrays of turbines implementing active yaw control is less established. For example, in the study of Fleming et al. [22], the Gaussian model proposed by Bastankhah et al. [21] was used together with the sum-of-squares (hereafter, SS) superposition method [33] to predict the wake flow of a wind farm with multiple yaw wind turbines, but it was found that there is a large difference between the model predictions and the LES results. A similar phenomenon also appeared in Ref. [23]. We believe that there are two reasons for the above deviation. First of all, the traditional wake superposition methods [33,34], represented by the SS used in Ref. [22], are all empirical formulas without solid theoretical foundation, and the only distinction is that the mathematical expressions are different. As pointed out by Crespo et al. [35], if not handled properly, it may bring about unrealistic results. Secondly, as aforementioned, vortex interactions can affect the wake steering performance, especially in cases with arrays of multiple turbines. However, in the common analytical wind farm models for active yaw control, their effects are not considered.

The above deficiency motivates the development of new models, and one of the representatives is the 3D analytical model proposed by Martínez-Tossas et al.[36]. Unlike the above-mentioned conventional 2D analytical models, it takes no assumption on wake shape, nor does it use superposition methods to describe the interaction effect of different wakes. Instead, it directly solves a linearized version of the Navier–Stokes momentum equation with the curl effect, which makes it to be able to capture the counter-rotating vortex pair in the wake flow of yawed wind turbines, and further, successfully reproduce the secondary wake steering effect on a downstream wind turbine. Despite of the merits, the available version of the 3D wake model is not mature enough at present, some important factors are not being taken into account, such as the vortex decay effect and the added turbulence generated by wind turbines. This results in some difference between the model prediction and the real yawed wake flow. Furthermore, the RANS-like implementation of the 3D wake model can increase the computation cost. Therefore, the 3D model is rarely used in engineering.

In contrast, although the conventional 2D wake models based on the geometrical deflection at hub height cannot reconcile all observed phenomenon, it should be admitted that researchers in the wind energy community have made a lot of efforts in that filed. They conducted a detailed and valuable analysis of the yawed wake flow in the hub height plane. Therefore, if some improvements are made to the existing analytical wind farm models based on the 2D models, for example, using a physical-based wake superposition method and modeling the vortex interactions in wake combination, the conventional analytical wind farm models may be revitalized. Fortunately, in a recent paper by Zong et al. [37], they derived a novel wake interaction model, rigorously from the law of conservation of momentum, referred to as "MC" model hereafter. It assumes that the total velocity deficit in the overlapped wake is equal to a weighted sum of the velocity deficit for each individual upwind turbine, rather than direct summation or square summation as in other common wake superposition methods without theoretical justification; and the weights are expressed as the ratio of the characteristic convection velocity of the individual wake to that of the overlapped wake. Additionally, following the momentum conservation in spanwise, the MC model has also been extended to combine the transverse velocity induced by yawed turbines, which make it possible to reproduce the secondary wake steering effect crucial to active yaw control.

Due to the advantages of the MC model, we believe that it is a good choice for simulating the superposed wakes of wind turbines operating in yawed conditions, although there is no relevant practice so far. What's more, to better characterize the effects of the transverse velocity induced by CPV in upstream yawed wakes, we introduce an "added yaw angle" to the wake-affected downstream wind turbines, and it is defined as the ratio of the "equivalent lateral velocity" to the

"equivalent streamwise velocity" within the rotor area. Combining the above modules with the Gaussian-based single wake model derived by Wei and Wan [32], a new analytical model for simulating wind farm wakes under yawed conditions is formed. To evaluate the performance of the newly proposed model, it is compared against a conventional wind farm model, where the most commonly used sum of squares operation is adopted to combine the wakes. Note that, in the conventional model, only the streamwise velocity of each individual wind turbine is superimposed, excluding the transverse velocity as no superposition principle is given; of course, the "added yaw angle" is also not considered. For validation purposes, lots of numerical simulations are performed, on two-turbine arrays and three-turbine arrays with different yaw angle distributions, using the SOWFA tool; and the obtained wind turbine wakes are used as a reference to evaluate the analytical model predictions. Moreover, for a quantitative assessment, we also sample the averaged wind fields at different downwind locations using several virtual turbines, and calculate their power productions. The regression analysis of the streamwise wake velocity is also included in our study.

The remainder of this paper is organized as follows. In Section 2, a new analytical model for predicting wind farm wakes under yawed conditions is proposed. Then, descriptions of numerical experiments performed by the SOWFA tool and related analysis methodologies are given in Section 3. By using the obtained LES wind field as a reference, in Section 4, the newly proposed model is evaluated and compared with a representative conventional analytical wind farm model. Finally, conclusions and future research are provided in Section 5.

2. Model description

In this part, a new method for modeling wind farm wake flows under yawed conditions is presented. Firstly, Section 2.1 briefly introduce the single analytical model applied to each wind turbine in the wind farm. Next, in Section 2.2, the wake superposition methods are given, used to describe the interaction mechanism of multiple wakes. In Section 2.3, an "added yaw angle" is defined for the downwind turbine operating in upstream yawed wakes. What's more, to close the analytical wind farm model, in Sections 2.4 and 2.5, methods used to estimate the local wake width growth rate and the aerodynamic performance of wind turbines are respectively illustrated in detail.

2.1. Single wake model

Due to the simplicity and the ability to reproduce various observations, in this study, the analytical wake model proposed by Wei and Wan [32] is adopted to predict the wake deflection and the far-wake velocity distributions for a single yawed wind turbine, including the streamwise velocity and the transverse velocity. It is a linear wake model derived from the conservation of mass and momentum, assuming the Gaussian profile for the streamwise velocity in the far-wake region.

In this analytical model, the equation for predicting streamwise velocity is written as:

$$\frac{u_w}{u_0} = 1 - \frac{C_T \cos\gamma}{16(k^* x/D + \varepsilon)^2} \times exp\left(-\frac{1}{2(k^* x/D + \varepsilon)^2}\left\{\left(\frac{z - z_h}{D}\right)^2 + \left(\frac{y - \delta}{D}\right)^2\right\}\right) \quad (1)$$

where x, y, and z are streamwise, spanwise, and vertical coordinates, respectively; u_0 is the local wind speed perceived by the wind turbine, D is the rotor diameter, z_h is the turbine hub height, δ represents the wake center deflection, C_T and γ respectively denote the thrust coefficient and yaw angle of the wind turbine. k^* represents the wake width growth rate, which should be specified in advance for using the above equation, and discussions related to its value estimation can be found in Section 2.4 below. ε is a model parameter, determined by:

$$\varepsilon = 0.2\sqrt{\beta} \quad (2)$$

where β is a function of C_T, given by:

$$\beta = \frac{1}{2}\frac{1 + \sqrt{1 - C_T \cos\gamma}}{\sqrt{1 - C_T \cos\gamma}} \quad (3)$$

What's more, the expression of the normalized wake center deflection is written as follows:

$$\frac{\delta}{D} = \theta_{c0}\frac{x_0}{D} + \frac{\sqrt{C_T/cos\,\gamma}\,sin\,\gamma}{23.866k^*} \times ln\left|\frac{\left(\frac{\sigma_0}{D} + 0.166\sqrt{C_T\,cos\,\gamma}\right)\left(\frac{\sigma}{D} - 0.166\sqrt{C_T\,cos\,\gamma}\right)}{\left(\frac{\sigma_0}{D} - 0.166\sqrt{C_T\,cos\,\gamma}\right)\left(\frac{\sigma}{D} + 0.166\sqrt{C_T\,cos\,\gamma}\right)}\right| \tag{4}$$

Note that Equation (4) is only applicable to the far-wake region for $x > x_0$,where x_0 represents the onset of the far wake. In the near wake area for $x < x_0$, the wake deflection is assumed to be linear with the downstream distance, i.e., $\delta = \theta_{c0}x$, and the initial skew angle θ_{c0} can be calculated by the approach of Coleman et al. [38]:

$$\theta_{c0} = \frac{0.3\gamma}{cos\,\gamma}(1 - \sqrt{1 - C_T\,cos\,\gamma}) \tag{5}$$

The normalized wake width at $x = x_0$ is determined by:

$$\frac{\sigma_0}{D} = \sqrt{\frac{C_T(sin\,\gamma + 1.978\,cos\,\gamma\,\theta_{c0})}{72\theta_{c0}}} \tag{6}$$

Based on the linear expansion assumption of the wake width, from Equation (6), result in:

$$\frac{x_0}{D} = \frac{(\sigma_0/D - \varepsilon)}{k^*} \tag{7}$$

Additionally, according to the relationship between the skew angle and wake velocity components, the transverse velocity in the far-wake region can be obtained, expressed as:

$$v = \frac{2.47C_T\,sin\,\gamma\,u_w}{72(k^*\,x/D + \varepsilon)^2 - 1.978C_T\,cos\,\gamma} \times exp\left(\frac{(y - \delta + \sigma)/D}{2(k^*\,x/D + \varepsilon)}\right)^2 \tag{8}$$

2.2. Wake superposition models

As illustrated in Introduction, the downwind turbine inside a wind farm can be affected by multiple wakes from several upstream turbines. Therefore, when calculating the wake velocity at a certain downwind turbine location, the cumulative wake effects are supposed to be taken into account.

In previous analytical wind farm models, the sum of squares(SS) superposition method [33] is commonly used to multiple wakes, in which, the total wake velocity deficit is assumed as follows:

$$U_w(x,y,z) = U_0 - \sqrt{\sum_j^N (u_0^j - u_w^j(x,y,z))^2} \tag{9}$$

where j loops through all the turbines involved, N is the total number of the upwind turbines whose wake have effects on the target place, U_0 is the inflow velocity of the wind farm, u_0^j is the wind speed experienced by the jth turbine and u_w^j is the wind velocity due to the single wake from the turbine j.

Note that although the SS model is only an experience-based superposition method without definite physical basis, this does not prevent its extensive application in literature and commercial software. Hence, the SS, as a representative of most of the previous works in wind farm power prediction[39,40], provides a reference for assessing the performance of the newly proposed model.

Additionally, for the newly proposed wind farm model in this study, the momentum conserving wake superposition method[37] is adopted to deal with the interaction of multiple wakes. To apply it, the mean convection velocity for each individual wake should be calculated at first, which represents the spatially dependent wake velocity in the whole wake cross-section and is determined by:

$$u_c(x) = \frac{\iint u_w(x,y,z) \cdot u_s(x,y,z)dydz}{\iint u_s(x,y,z)dydz} \tag{10}$$

where u_s is the individual velocity deficit, defined as $u_s = u_0 - u_w$; and u_w is the corresponding streamwise velocity, can be calculated with Equation (1).

From Equations (1) and (10), yield:

$$\frac{u_c(x)}{u_0} = 1 - \frac{1}{\sqrt{2}} \times \frac{C_T \cos\gamma}{16(k^* x/D + \varepsilon)^2} \tag{11}$$

Following a similar procedure as the individual wake, the mean convection velocity for the overlapped wake (denoted by U_c) is defined as follows:

$$U_c(x) = \frac{\iint U_w(x,y,z) \cdot U_s(x,y,z)dydz}{\iint U_s(x,y,z)dydz} \tag{12}$$

where U_w is the combined wake velocity, given by:

$$U_w = U_0 - U_s \tag{13}$$

where U_s is the total velocity deficit in the superposed wake. To conserve the total momentum deficit in the streamwise direction during wake superposition, it has to satisfy the following expression:

$$U_s(x,y,z) = \sum_j^N \frac{u_c^j(x)}{U_c(x)} u_s^j(x,y,z) \tag{14}$$

Obviously, to solve U_c out of Equations (12) and (14), iterative calculations should be performed. Specifically, at first, assuming that U_c is equal to the maximum value of u_c^j, and then, estimate the total velocity deficit according to Equation (14); next, substitute the obtained U_s into Equation (12), to get the corrective value of the mean convection velocity for the combined wake U_c^*; at last, let $U_c = U_c^*$, and repeat the above steps until the convergence criterion is met. In Zong et al.[37], the criterion is set to $|U_c - U_c^*|/U_c^* \leq 0.001$, which is also adopted in the present work. Under such condition, the calculation can usually reach convergence within 5 iterations.

Analogous to Equation (14), following the momentum conservation in the spanwise direction, the total transverse velocity for the combined wake can be written as：

$$V(x,y,z) = \sum_j^N \frac{u_c^j(x)}{U_c(x)} v^j(x,y,z) \tag{15}$$

where v^j is the transverse velocity of the jth single wake, it can be found by Equation (8).

2.3. Definition of the "added yaw angle"

In order to better reflect the effects of transverse velocity induced by CPV in upstream yawed turbine wakes, a virtual "added yaw angle" is defined for the wake-affected downstream wind turbine, as shown in Figure 1. This is understandable since the upstream transverse velocity does change the local wind direction perceived by the downwind turbine. Therefore, when applying the single analytical model described in Section 2.1, a hypothetical yaw angle should be attached to the downwind turbine that overlaps with the upstream yawed wakes.

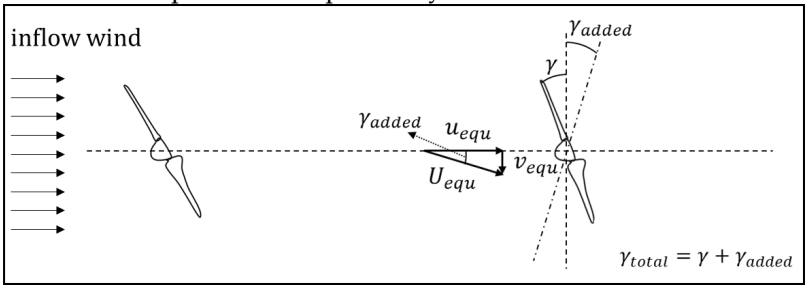

Figure 1. Schematic diagram of the "added yaw angle".

The "added yaw angle"(γ_{added}) is defined as an angle between the incoming wind direction and the equivalent resultant velocity (U_{equ}) acting at the rotor plane, it is composed of the equivalent transverse velocity(v_{equ}) and the equivalent streamwise velocity(u_{equ}), as presented in Figure 1. Specifically, in the calculation, first designate a number of sampling points in the rotor disk; then, extracting the wake velocity in each point and taking the average, thereby, the aforementioned equivalent values can be obtained:

$$u_{equ} = \sum_{k}^{M} u_k /M \tag{16}$$

$$v_{equ} = \sum_{k}^{M} v_k /M \tag{17}$$

$$U_{equ} = \sqrt{u_{equ}^2 + v_{equ}^2} \tag{18}$$

$$\gamma_{added} = arctan(v_{equ}/u_{equ}) \tag{19}$$

$$\gamma_{total} = \gamma_{set} + \gamma_{added} \tag{20}$$

where k is the index number, u_k and v_k are respectively the values of the streamwise and transverse wake velocity components at the kth point, they can be obtained by Equations (13) and (15); M is the total number of sample points. γ_{total} and γ_{set} in Equation (20) correspond to the total yaw angle perceived by the wind turbine and its set yaw value.

For the sake of clarity, Figure 2 shows a flow chart for modeling multiple wind turbine wakes under yawed conditions with the above-mentioned modules. The specific operations, in the order of execution, are described as follows. (1). Firstly, sort the wind turbines according to their relative locations along the inflow direction; (2). Starting the calculation from the most upstream turbine, apply the single analytical model to calculate the wake velocity components and the mean convection velocity for the individual wake at each downwind location; (3). In light of Equations (18) and (20), estimate the equivalent resultant velocity and the total yaw angle for the immediately adjacent downwind turbine; (4). Inserting the obtained values into the single wake model again, to predict the wake characteristics of the aforementioned downwind turbine in stand-alone conditions; (5) Deploy an iterative method to solve the mean convection velocity for the combined wake out of Equations (12) and (14), and then, by substituting the calculated U_c into Equations (14) and (15), the total streamwise velocity deficit and the total transverse velocity can be obtained. Obviously, this lay a foundation for predicting U_{equ} and γ_{total} of further downstream wind turbines; (6). Repeat steps 3 to 5 until the last wind turbine, thus completing the wake modeling of the whole wind farm.

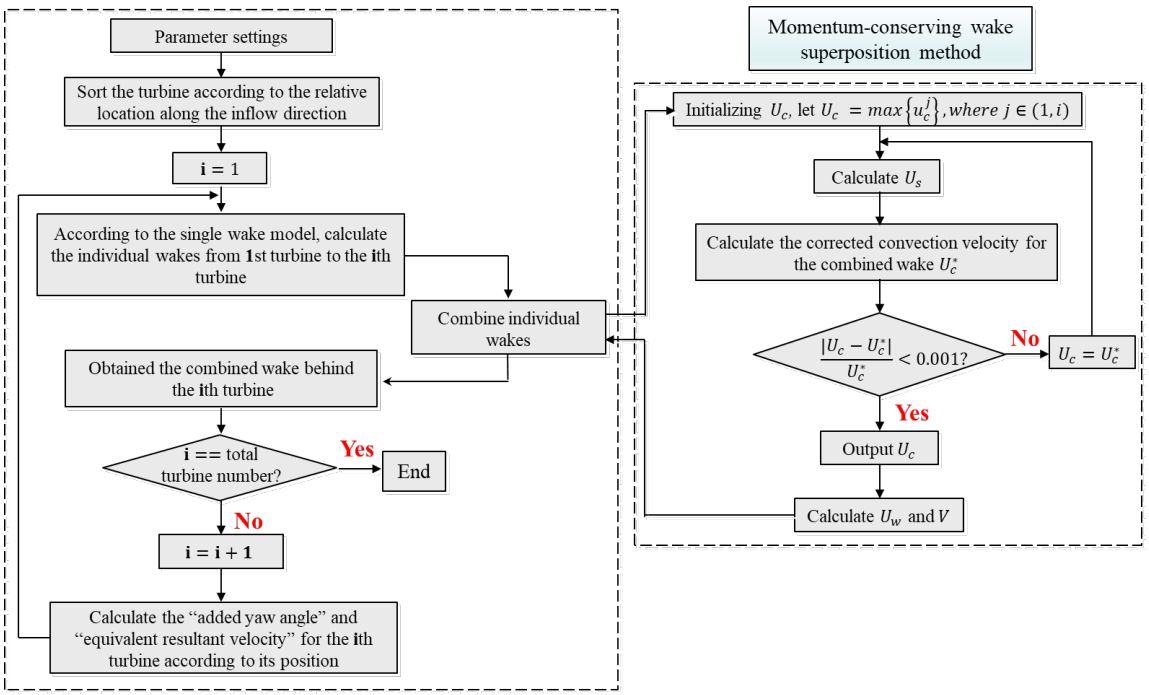

Figure 2. Flow chart for modeling multiple wind turbine wakes under yawed conditions using the newly proposed model.

2.4. Turbulence intensity Model

For a wind turbine located in the combined wake of multiple upstream turbines, the local turbulence intensity it perceived includes not only the ambient turbulence intensity component, but also that generated by upwind turbines, referred to as "added turbulence intensity"[41,42]. What's more, the wake width growth rate k^* in Equation (1) is known to be strongly affected by the turbulence intensity level [43]. Therefore, in order to better characterize the turbulence effects and improve the accuracy of wind farm power prediction, in here, following the work of Niayifar et al.[44], the wake width growth rate is no longer assumed to be constant, but expressed as a function of the local turbulence intensity at the wind turbine.

$$k^* = k_a \cdot I + k_b \tag{21}$$

where k_a and k_b are tuning parameters, and I is the local streamwise turbulence intensity immediately upstream of the target wind turbine. Note that, Equation (21) has been widely used in wind farm wake predictions [37,45] and achieved good results.

As illustrated above, the local streamwise turbulence intensity in the cumulative wake flows can be decomposed into two parts, given by:

$$I = \sqrt{I_0^2 + I_+^2} \tag{22}$$

where I_0 is the ambient turbulence intensity, I_+ is the added turbulence intensity induced by wind turbines.

For modeling I_+ in the far wake region, researches in the wind energy community have proposed several empirical equations [46,47]. In the internal tests, the Frandsen model [47] is found to be able to well simulate the mean added turbulence intensity after 5D downstream of the yawed wind turbine, and it is simple in form and has few input parameters. Consequently, in the present work, the Frandsen model is chosen to estimate the added turbulence intensity generated by wind turbines, it is expressed as:

$$I_+ = \sqrt{KC_T}/(x/D) \tag{23}$$

where K is a constant, set to 0.4.

In addition, from Ref.[44,48], the local turbulence intensity faced by a downwind turbine in the wind farm is largely affected by its surrounding upstream turbines, and the following method[44] is frequently used to calculate the added turbulence intensity at a given wind turbine (assuming its index number is i):

$$I_{+i} = max\left(\frac{A_w 4}{\pi D^2} I_{+ji}\right) \tag{24}$$

where I_{+i} is the added turbulence intensity perceived by the target turbine i, I_{+ji} is the added turbulence intensity generated by the upstream turbine j at the target turbine i, $\pi D^2/4$ and A_w are respectively the rotor area of turbine i and the overlap area between the ith turbine rotor plane and the wake of the jth turbine.

To calculate A_w in Equation (24), according to Niayifar et al.[44], a top-hat profile with a diameter of 4σ is assumed for the added turbulence intensity distribution, where σ is the standard deviation of the Gaussian-like velocity deficit profile, which is widely used as the characteristic wake width in previous studies[28,31,43].

2.5. Turbine model

As indicated by Equation (1), the thrust coefficient is an important input of the single wake model; power production is also a key indicator of the turbine performance. Hence, apart from the wake modeling module used to describe the wake characteristics, the wind turbine model should also be incorporated into the analytical wind farm model. Under non-yawed conditions, it is a common practice to plot the power and thrust coefficient curves as a function of the effective wind speed at the rotor, to predict the power production and thrust force corresponding to the local conditions the wind turbine is operating in [49,50].

The turbine used in the present work is the NREL 5-MW wind turbine, which is a three-blade upwind turbine with a rotor diameter of 126 m and a hub height of 90 m, and the reader can refer to Jonkman et al. [51] for more details on it. Additionally, the power and thrust coefficient curves of the NREL 5-MW turbine are shown in Figure 3. Note that the drawing data are derived from internal numerical simulations, may be slightly different to the results calculated by FAST [52], as only the rotor blades are modeled in the simulations, excluding tower and nacelle.

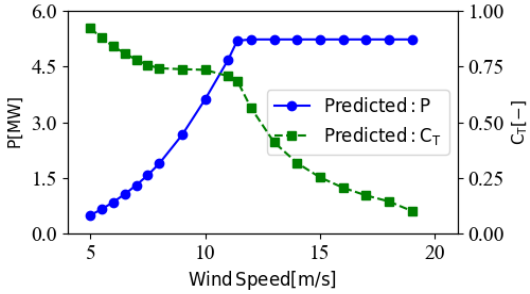

Figure 3. Simulated power and thrust coefficient curves with respect to the wind speed for the NREL 5-MW wind turbine.

When the wind turbine yaws, due to the reduction in the effective inflow speed and the rotor frontal area, a drop is seen in power output and thrust force [8,9,10,53]. Therefore, in order to accurately predict the power and thrust of the yawed wind turbine, it is important to establish a reliable model to reflect the effect of yaw on the aerodynamic performance, and researchers have done lots of relative studies. For example, in actuator disk theory [54], assuming that only the normal velocity component crosses the rotor plane. For a yawed wind turbine, the axial inflow component it perceives is quite different from that of a non-yawed turbine, and in geometric, the two are in a cosine relationship, so:

$$P = P_0 \cdot cos^3\gamma \tag{25}$$

$$T = T_0 \cdot cos^2\gamma \tag{26}$$

where P and T denote the power and thrust force under yawed conditions; P_0 and T_0 are the power and thrust force at zero yaw.

However, it should be mentioned that multiple factors can affect the performance of the yawed turbine, for instance, the turbine type and operating conditions [10,53]. Consequently, the above relationships have not been widely recognized, although they are supported by some experimental results [55]. Additionally, in the Ref. [10,56], it was observed that the power of a yawed turbine was proportional to the square of cosine of yaw angle; and in Zong et al. [9], a $cos^{1.8}\gamma$ shape was found to fit the $C_T - \gamma$ curve. In conclude, it is difficult to find unanimous statement about the relationships between power, thrust and yaw angle.

To achieve the goal of accurately predict the steady-state aerodynamic performance of a yawed wind turbine at different operating conditions, Dahlberg and Montgomery [57] proposed the following method, in which, tunable parameters are introduced to match the power and thrust loss caused by yaw:

$$P = P_0 \cdot cos^p\gamma \tag{27}$$

$$C_T = C_{T0} \cdot cos^q\gamma \tag{28}$$

where C_{T0} represents the thrust coefficient at zero yaw; p and q are tunable parameters.

Due to the flexible of the Dahlberg's method, it is adopted in the present work, and the values of the tunable parameters are determined by fitting the numerical simulation data for the NREL 5MW wind turbine at different yaw angles. More details are shown in Section 4.1 below.

3. Wake simulations

To assess the performance of different analytical wind farm models for active yaw control, a number of numerical simulations for wind turbines with different yaw angle distributions are performed using the SOWFA tool, and the obtained LES wind field is used as a reference. The numerical setting of the test cases is described in Section 3.1, and then, some analysis methods for assessing analytical model predictions are given in Section 3.2.

3.1. Numerical setup and test cases

The numerical simulations are conducted using the Simulator for Wind Farm Applications (SOWFA) from the National Renewable Energy Laboratory (NREL), which is a high-fidelity tool for investigating the wind turbine performance and wake characteristics. Within SOWFA, the LES technique is applied to solve the filtered Navier–Stokes equations, and the contribution of the sub-grid scales to the resolved flow field is parameterized by the eddy-viscosity model. In particular, the governing equations are discretized using an unstructured, collocated, finite-volume formulation, and the time discretization is second-order backward. Additionally, the actuator line method [58] is introduced to model the turbine-induced forces for improving computational efficiency, which was widely used in previous and its effectiveness has been validated [5,28]. More details on the SOWFA tool can be found in Ref. [59].

In the current study, at first, several numerical simulations on a single wind turbine are conducted, with the yaw angle being 0°, 10°, 20° and 30°, respectively. Next, to provide a reference wind field for the analytical model predictions, four test cases are considered, including three two-turbine arrays and a three-turbine array, where the streamwise spacing between two consecutive turbines is 7 rotor diameters. In the test cases one, two and three, the first wind turbine is operating with 10°, 20° and 30° yaw misalignment, respectively; and the second turbine is maintained non-yawed. In the fourth case, three tandem-arranged wind turbines are tested, with the most upstream turbine being yawed 20°. What's more, to evaluate the predictive performance of analytical models on power output, another several two-turbine scenarios are simulated where the front turbine is yawed 20° and the yaw angle of the second turbine is varied through a range of -15° and +15°.

Specifically, the numerical simulation of each test case is divided into two stages. Firstly, a precursor simulation without wind turbines is performed to generate a realistic neutral boundary layer(NBL). The computational domain size is 3000 m×3000 m×1000 m, and it is discretized into 300×300×100 grid points. All lateral boundaries in this simulation stage are periodic, and the horizontally mean wind speed at turbine hub height is driven to 8 m/s. What's more, the surface aerodynamic roughness height and the potential temperature rate are respectively set to 0.001 m and 0 K/m, typical of the offshore conditions. In a whole, the setting is the same as that in Ref. [59], because the inflow it generates has been validated and represents a realistic scenario. The precursor simulation first ran for 18000 s, to ensure reaching a quasi-steady condition; and then, it ran for another 2000 s, and during that time, the relevant flow variables on the upstream boundary were stored at every time step, which would be enforced as the inflow boundary condition in the next simulation stage.

In the second stage, the wind turbines are immersed in the flow field. The boundary conditions in this simulation stage are different from the precursor simulation. In particular, only the side boundaries are periodic; for the upstream boundary condition, it is specified using the saved plane of turbulent data; and on the downstream boundary, the gradient of velocity and temperature are taken to be zero so that the turbine-induced wakes can exit without cycling back. What's more, we locally refined the mesh around the wind turbines and their wakes so as to gain the resolution required to capture the wake structures. Details on the positioning of the turbine and meshing of the domain are presented in Figure 4. For each test case, the second stage simulation ran for 2000 s, but only the simulated data in the last 1200 s was extracted and averaged to eliminate the transient effects. Moreover, it should be mentioned that, in order to exclude the additional wake deflection arising from the vertical momentum, no vertical tilt is applied to the turbine rotor in the numerical simulations, although in fact, the NREL 5-MW wind turbine used in the present work has a 5° shaft tilt to avoid the blade-tower collision.

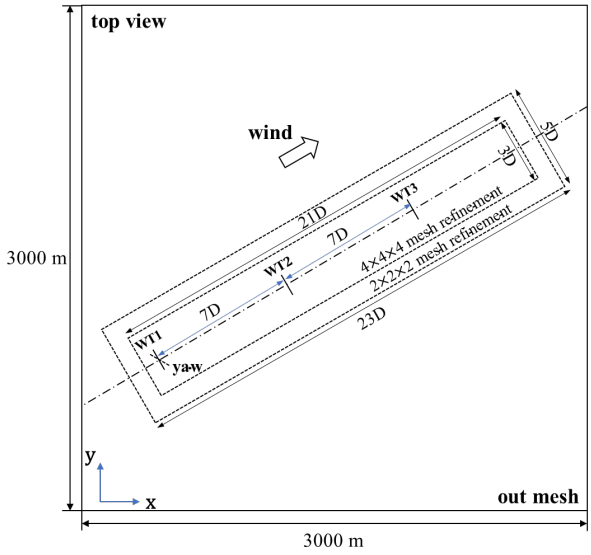

Figure 4. Schematic on the positioning of the turbine and meshing of the domain. D represents the rotor diameter. WT1, WT2, and WT3 are the names of wind turbines.

Figure 5 presents the statistical features of the inflow generated in precursor simulation stage. The vertical profiles of the normalized streamwise inflow velocity and the streamwise turbulence intensity are shown in Figure 5(a) and (b). It can be seen that, the mean incoming wind speed and the turbulence intensity at hub height are around 8 m/s and 5.6%, respectively. In addition, to further assess the simulated boundary layer flow, we plot the measured streamwise velocity profile and the perfect logarithmic velocity profile on a semi-log scale in Figure 5(c). Apparently, below approximately 100 m, corresponding to the position of $z/D = 10^0$ in the x label, the measured inflow velocity profile substantially satisfies the law of the wall scaling, indicating that the desired inflow condition can be well generated in the precursor simulation.

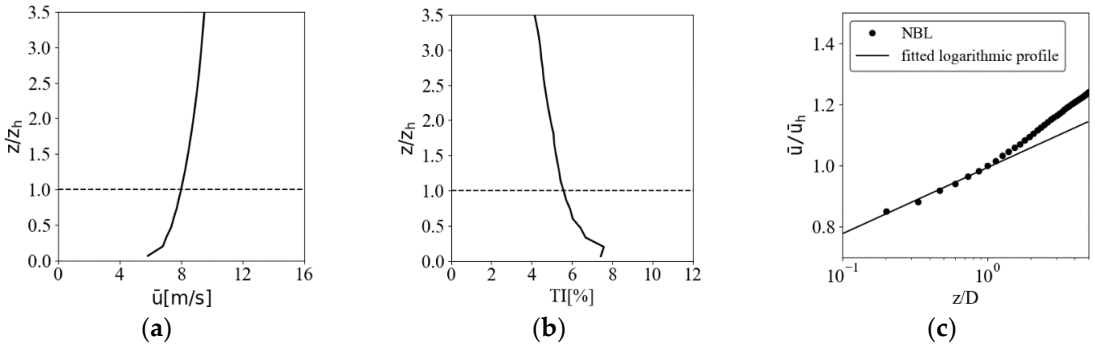

Figure 5. Main features of the incoming flow: vertical profiles of (a) the normalized streamwise inflow velocity and (b) the streamwise turbulence intensity. The horizontal dashed line indicates the hub height level; (c) vertical profile of the normalized streamwise inflow velocity on a semi-log scale. The black solid line represents perfect law-of-the-wall scaling.

3.2. analysis methods

In order to better evaluate the performance of different wind farm wake models, we introduce two analysis methods in the present work. The first one is the linear regression analysis. To be specific, based on the wake flow data obtained from both the LES wind field and the analytical model, we can get a fitted regression line reflecting their relationship. According to the slope A and intercept B of that regression line, the correlations between the reference wind field and model prediction can be well examined, where the ideal values of A and B are 1 and 0, respectively.

Secondly, a similar approach to Vollmer et al. [19] is adopted to sample the wake flow data at different downwind locations in the superposed wake area, using virtual wind turbines of the same type as in the numerical simulations. The difference from Vollmer et al. [19] is that the method is no longer used to identify the wake center, but focuses on predicting the power generation of the hypothetical wind turbine at the given downwind location. The virtual turbine rotors are arranged as shown in Figure 6. For different test cases, they sweep across the wake area behind the second or third wind turbine, which makes it possible to calculate the continuous change in power output of the downwind turbine. In particular, for a virtual wind turbine placed at a given downwind location, its normalized available power can be obtained by averaging the cubed wind speed over a circular plane with a diameter of D centered around the turbine hub height, based on the extracted wake flow data:

$$P_{av}^{*} = \frac{\int 0.5\rho u_w^3 dA}{\int 0.5\rho u_0^3 dA} \tag{29}$$

With the above definition, if there is a real wind turbine in that given location, the normalized power it generated is equal to P_{av}^{*} multiplied by the power coefficient C_P. In this way, the ability for a wide variety of turbine array configurations to extract wind energy can be well quantified, regardless of whether the downstream turbine experiences full-wake or partial-wake conditions. Therefore, it is useful for assessing the predictive performance and universality of wind farm wake models.

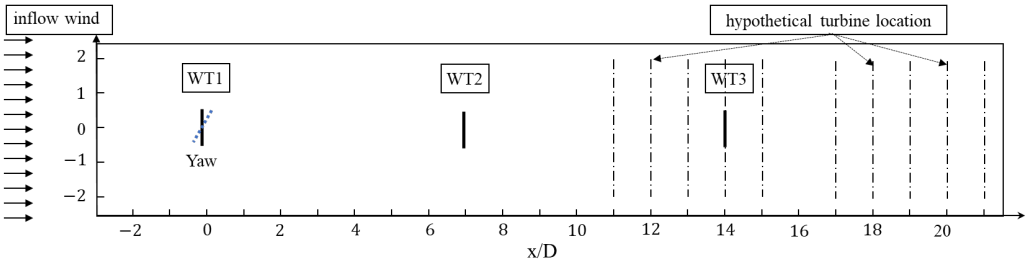

Figure 6. Illustrative sketch of the distribution of virtual turbines used to evaluate the performance of analytical models. The black solid lines represent the positions of the real wind turbines, and the black dots denote the locations of the virtual turbines.

4. Results and discussions

In Section 4.1, the wake characteristics and aerodynamic coefficients for a single wind turbine at different yaw angles are analyzed, with the purpose of determining the unknown parameters in the newly proposed model and performing a priori calibration of the performance of the sub-modules. Then, in Section 4.2, the wake fields obtained from the new proposed model and the conventional analytical wind farm model are compared against the LES results for different test cases. Additionally, since the main objective of active yaw control is to maximize the total power production of wind farm, in Section 4.3, the change in power gain of downstream wind turbines at different yaw angle distributions are evaluated and discussed.

4.1. single turbine scenario

Firstly, we examine the accuracy of large eddy simulations conducted by the SOWFA tool. In Figure 7, the mean streamwise velocity deficit profiles under non-yawed conditions obtained from the present LES are compared with the result of Churchfield et al.[59], which is widely accepted and cited. In their works, the wake flow behavior and the aerodynamic performance of the NREL 5-MW wind turbine were studied under the same inflow condition as the current simulation. As evident in Figure 7, the LES data in the current simulation agrees well with that from Churchfield et al.

Considering that in all numerical experiments in this work, except for the yaw angle distribution and the number of wind turbines, other settings, such as the computational domain, boundary conditions, inflow condition, mesh resolution, time step, are all the same. Consequently, according to the aforementioned comparison for the wake of a single wind turbine at zero-yaw, it is reasonable to acknowledge that the LES results of the wind turbine wake in the current work are accurate. This indicates that the LES wind field can be used as a reference to evaluate the analytical model predictions.

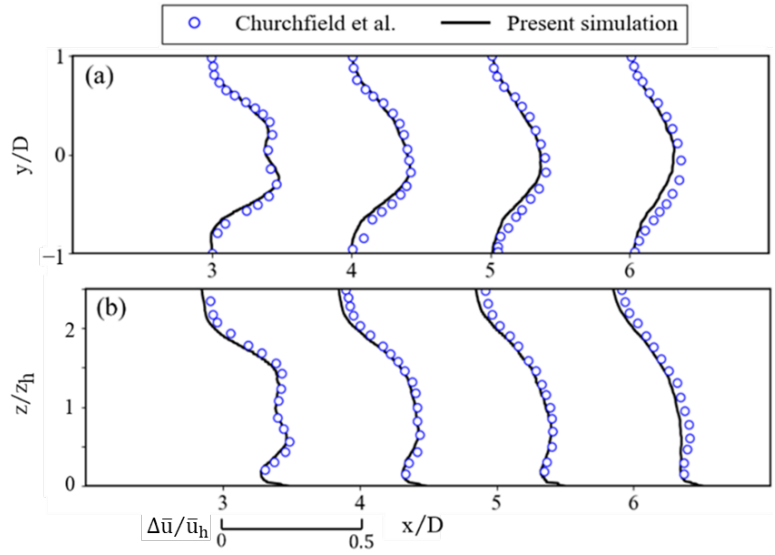

Figure 7. Profiles of the normalized mean streamwise velocity deficit in (a) the horizontal hub-height plane and (b) the vertical plane normal to the wind turbine under non-yawed conditions.

Next, in Figure 8, the predicted values of I at x=7D downstream of the wind turbine are compared against those obtained from large eddy simulation (LES). The reason for choosing this configuration is that, for all test cases with multiple turbines in the current work, the inter-turbine spacing is fixed at 7 rotor diameters. As apparent in Figure 8, the method of Niayifar et al. [44], described in detail in Section 2.4, can provide a good prediction of the streamwise turbulence intensity at different yaw angles.

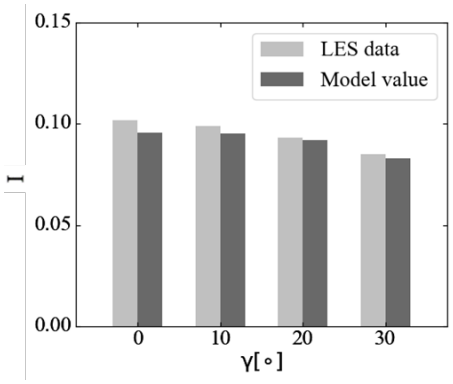

Figure 8. Values of the local streamwise turbulence intensity at x = 7D behind a single wind turbine for different yaw angles. The grey bars indicate the LES data and the black bars denote the model predictions.

In Figure 9, the wake width growth rate behind the NREL 5-MW wind turbine is plotted as a function of the streamwise turbulence intensity at hub height. It is shown that the k^* value does change approximately linearly with I, as assumed by Equation (21). Additionally, from the fitted line of the simulated data, k_a and k_b in Equation (21) are determined to be 0.32 and 0.002, respectively.

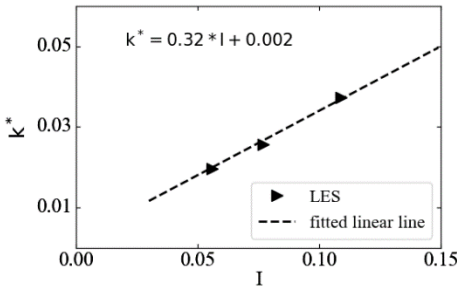

Figure 9. Variations in wake width growth rate for the NREL 5-MW wind turbine with the streamwise turbulence intensities at hub height.

To calibrate the settings of k_a and k_b, here we compare the LES results for a single wind turbine at different yaw angles to the predictions of the new proposed model (note that, since only a single turbine is considered, the new model is equivalent to the single wake model derived by Wei et al.[32]). In particular, with k_a= 0.32, k_b= 0.002 and I=0.056, the wake width growth rate for the wind turbine is k^*= 0.02, which is around the same as the suggested value in Ref.[32]. Figure 10 presents lateral profiles of the normalized mean streamwise velocity deficit at different downwind locations. Obviously, good consistency is found between the proposed model predictions and the LES data for different yaw angles, indicating that the current settings of k_a and k_b are reasonable. This also lays the foundation for further applying the new proposed model to simulate multiple wind turbine wakes under yawed conditions.

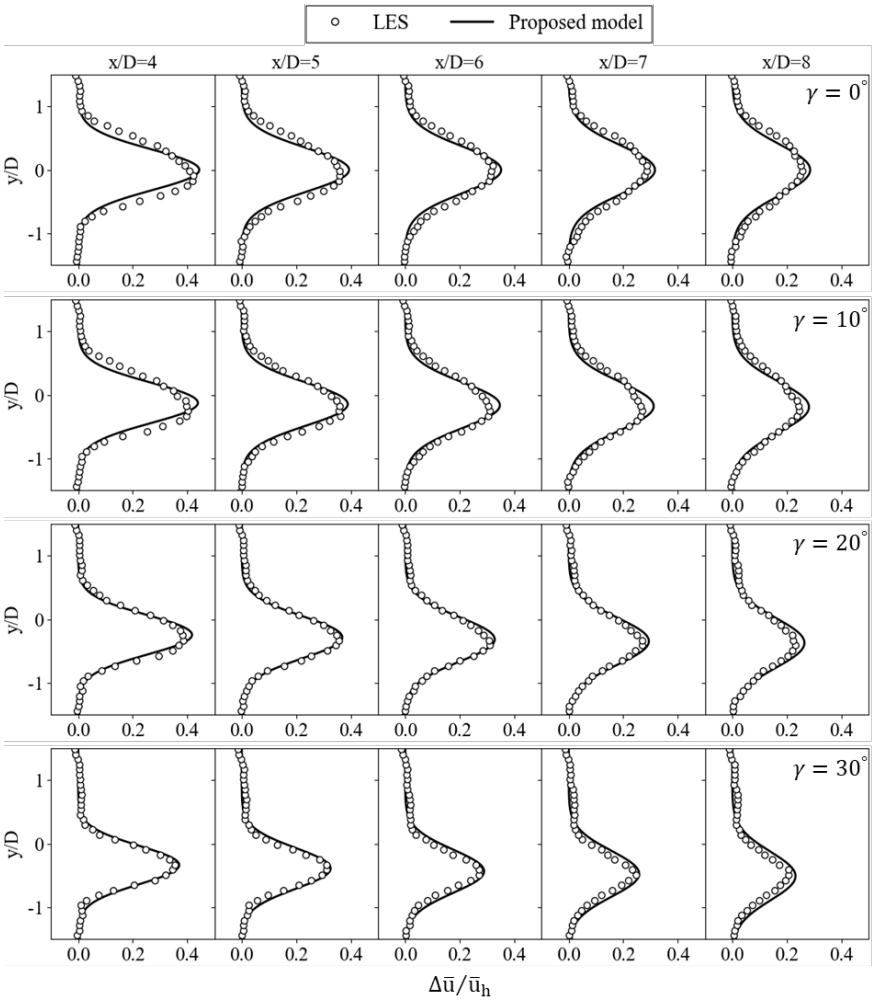

Figure 10. Lateral profiles of the normalized streamwise velocity deficit in the wake of a turbine with γ=0°, 10°, 20° and 30° : LES data (open circle) and new proposed model (black solid line)

What's more, as illustrated in Section 2.5, to give the aerodynamic performance of a wind turbine under yaw misalignment conditions, the cosine exponents p and q in Equations (27) and (28) should be determined. Following the approach of Dahlberg et al. [57], we in Figure 11 plot the power and thrust coefficients of the NREL 5-MW wind turbine at different yaw angles, and normalized them by their maximum values at $\gamma = 0^{\circ}$,respectively. It can be seen that in our numerical simulations, the normalized power production approximately varies as $cos^{1.92}\gamma$, and C_T versus γ has a shape similar to $cos^{1.19}\gamma$.

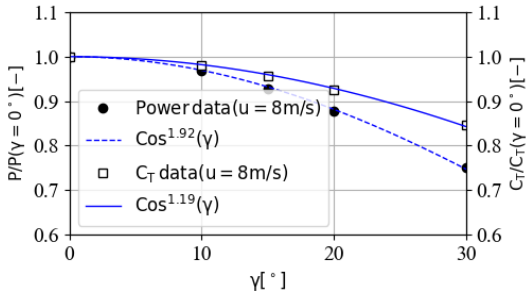

Figure 11. Changes in the normalized power production and thrust coefficient of the NREL 5-MW wind turbine for different yaw angles. Black circles/squares correspond to the simulated data and the blue solid/dashed line represent Cosine fits.

4.2. multiple-turbine wake analysis

4.2.1 Test case 1(two aligned wind turbines with the front one being yawed 10°)

The two-turbine array displayed in Figure 12 is the first test case, in which the front wind turbine yaws by 10°. As presented, when the first turbine operates with a small yaw angle, the wake width and streamwise velocity deficit in the overlapped wake are under-predicted by the conventional analytical model. Oppositely, an over-estimated velocity deficit is shown in the predictions of the new model, especially in the near-wake. However, as the wake going downstream, the new proposed model predictions gradually converge to the LES data, and in a whole, compared to the conventional model, the new proposed model provides a better prediction result.

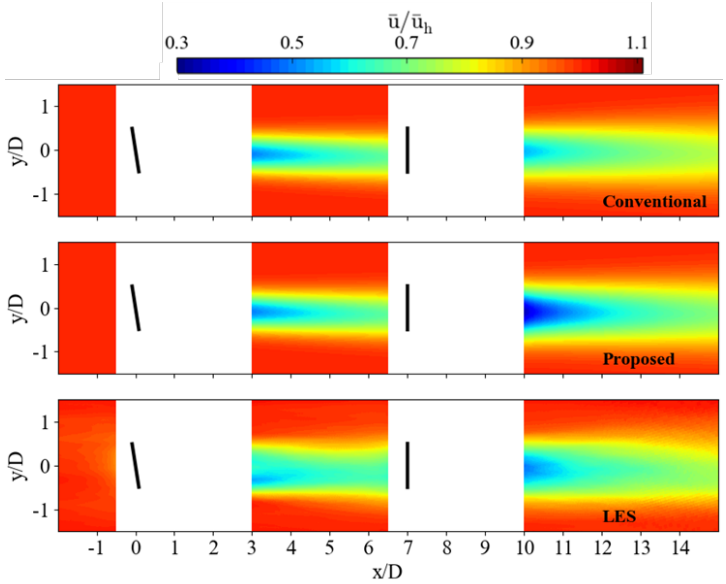

Figure 12. Contours of the normalized streamwise velocity in the horizontal hub-height plane for two aligned wind turbines when the front turbine is yawed 10°: Conventional analytical model(top), new proposed model (middle) and the large-eddy simulations (bottom).

To further evaluate the difference between the LES flow field and the model predictions, we in Figure 13 compare the lateral profiles of the normalized streamwise velocity deficit behind the second wind turbine, at the chosen downwind locations (x=11D, 12D, 13D, 14D, 15D). Similar to the above analysis, the conventional model using the sum of squares superposition method is found to underestimate the velocity deficit, and more seriously, it fails to capture the "secondary wake steering". For the newly proposed model, it exhibits some biases towards overestimating the velocity deficit with respect to the reference wind field, obvious before x/D=12, but as the wake develops further downstream, the situation is greatly improved. The above departure occurs in the physical-based new model may be attributed to the limitation of the single wake model[19] used, which is developed for far wake modeling and some assumptions it adopted are only applicable to the fully developed wakes.

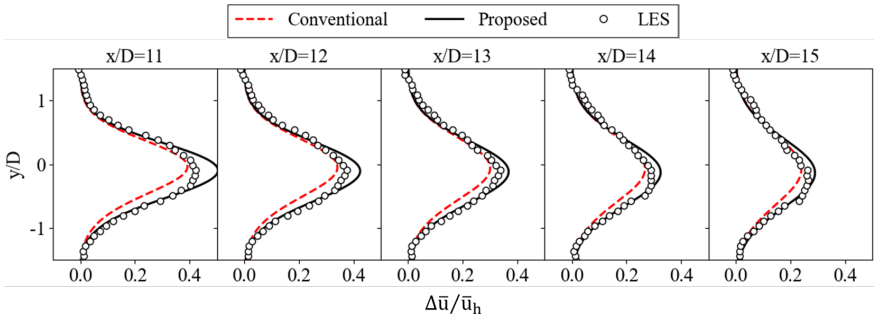

Figure 13. Lateral profiles of the normalized streamwise velocity deficit in the wakes at different downwind locations behind the second turbine when the front turbine is yawed 10°: LES data (open circle), new proposed model (black solid line), and conventional analytical model (red dashed line).

What's more, we also perform regression analysis on the streamwise velocity at different cross-sections, and the results is shown in Figure 14. The x-axis and y-axis in the plot represent the streamwise wake velocity extracted from the large eddy simulation and predicted by the analytical model, respectively. The black diagonal line indicates the two are equal to each other. As mentioned above, compared with the reference wind field, the predictions of both analytical models have large errors in the combined wake near the second wind turbine, especially in the wake center region. The distinguish is that the velocity deficit is overestimated by the new model while it is under-predicted by the conventional model. As such, the intercept of the regression line is large for both models. However, in contrast, the absolute value of the intercept for the new model is only about half of that for the conventional model, indicating that the new model performs a little better. Additionally, one can also observed that, the slope of the regression line for the new proposed model is also relatively closer to the ideal value, this is due to the fact that the new model can reasonably predict the wake deflection in the overlapped wake, and at further downstream positions, the deviation of its predicted streamwise velocity from the reference wind field becomes smaller.

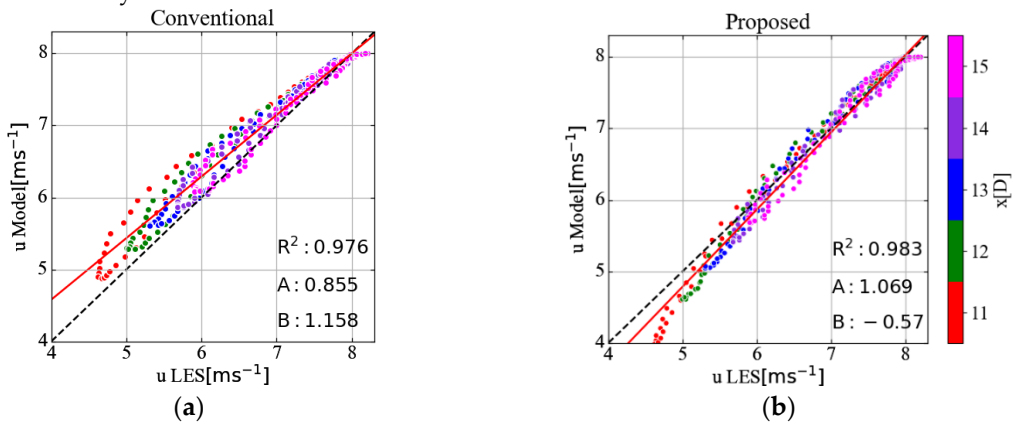

Figure 14. Scatter plot and corresponding regression line of the streamwise wake velocity as predicted using (a) the conventional analytical model and (b) the new proposed model, in relation to the reference wind field calculated with large-eddy simulations (LESs).

Since the main interest for implementing active yaw control is to seek optimal power production of the entire wind farm, accurately predict the power output of wind turbines is important for analytical wake models. As shown in Figure 15, the normalized available power of virtual wind turbines located behind the second turbine are computed, sweeping the spanwise direction of the wake flow at several downwind locations. It is apparent that there is a substantial difference between the conventional model predictions and the LES data. To be specific, in LES, the "profile" of power deficit is further deflected with respect to the incoming steered wake. However, the conventional model shows that the power deficit "profile" only shifts slightly as the wake traveling downstream, this is because no effect of the transverse velocity induced by upstream yawed turbine is considered. On the contrary, the new proposed model agrees well with the LES data except at the edge of the wake, demonstrating the potential of applying it to predict the wake steering performance.

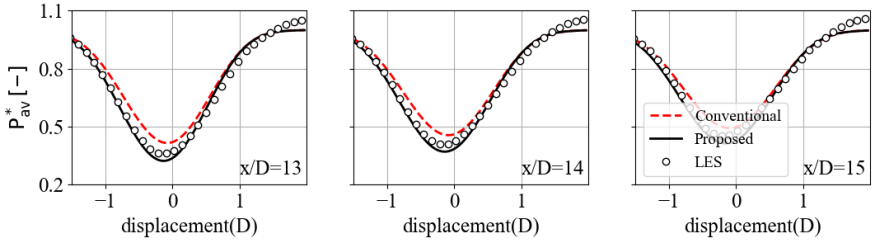

Figure 15. Power production of a hypothetical turbine behind the second turbine when the front turbine is yawed 10°: LES data (open circle), new proposed model (black solid line), and conventional analytical model (red dashed line).

4.2.2 Test case 2(two aligned wind turbines with the front one being yawed 20°)

Next, take a look at another two-turbine array with the upstream turbine being yawed 20°. Figure 16 shows the contours of the normalized streamwise velocity in the horizontal plane at hub height. As seen in the SOWFA case, due to a larger yaw angle of the front wind turbine, the "secondary wake steering" phenomenon in the overlapped wake becomes more obvious. In addition, some disparities occur between the LES results and the conventional model, which cannot predict the continuous deflection of the wake behind the second wind turbine. In contrast, the newly proposed model well captures the flow characteristics of the combined wake.

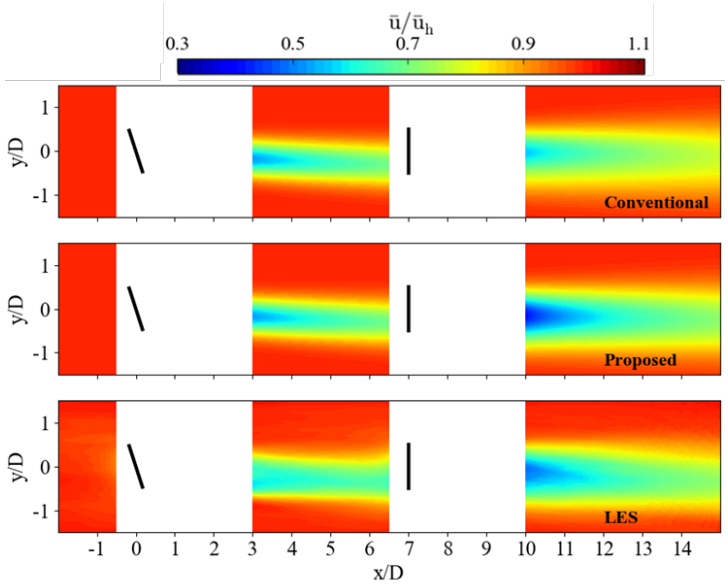

Figure 16. Contours of the normalized streamwise velocity in the horizontal hub-height plane for two aligned wind turbines when the front turbine is yawed 20°: Conventional analytical model(top), new proposed model (middle) and the large-eddy simulations (bottom).

Figure 17 presents the development of the horizontal profiles of the normalized streamwise velocity deficit at different downwind distances. As shown in the SOWFA case, with increasing yaw angle of the front wind turbine, the second turbine's wake appears to deflect larger, which is consistent with the above analysis. What's more, good agreement is found between the LES data and the predictions of the new model. As for the conventional analytical model, it underestimates the velocity deficit in the superposed wake area, and does not capture the “secondary wake steering” phenomenon. This is because in the conventional model, the impact of the front turbine wake on the downstream wind turbines mainly includes reduced velocity and increased turbulence intensity (reflected by the change in wake width growth rate). Obviously, neither of these two effects can cause the additional deflection of the downwind turbine wake.

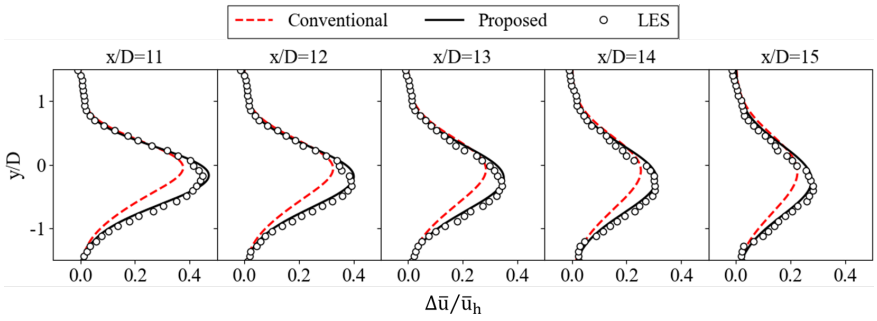

Figure 17. Lateral profiles of the normalized streamwise velocity deficit in the wakes at different downwind locations behind the second turbine when the front turbine is yawed 20°: LES data (open circle), new proposed model (black solid line), and conventional analytical model (red dashed line).

The results of the regression analysis for Test case 2 are collected in Figure 18. According to the slope A and the intercept B, we can see that the new analytical model is close to a perfect regression line. However, these terms in the conventional model don't show good results, which can be explained as follows: At each selected downwind position, the maximum velocity deficit in the wake center region is under-estimated, as presented in Figure 17; In addition, the conventional model cannot capture the "secondary wake steering" effect, so the deviation between its predictions from the reference wind field becomes more larger as the wake moving sideways, especially in the wake steering direction. Consequently, the regression line for the conventional model has a higher intercept and a lower slope.

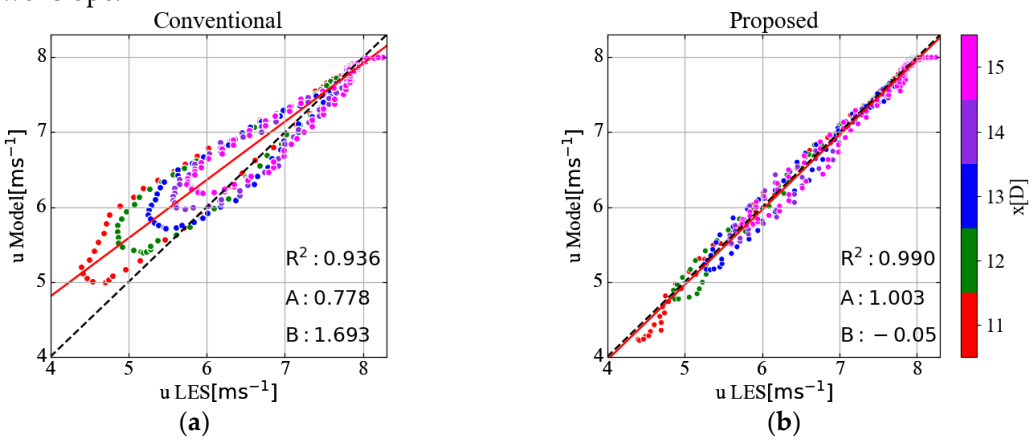

Figure 18. Scatter plot and corresponding regression line of the streamwise wake velocity as predicted using (a) the conventional analytical model and (b) the new proposed model, in relation to the reference wind field calculated with large-eddy simulations (LESs).

To further explore the difference in wake predictions by the two analytical models, power outputs of virtual turbines are calculated, and the results are displayed in Figure 19. Apparently, the new proposed model shows better performance than the conventional model by closely following the power profile of the reference case. What's more, as expected, due to the failure to capture the "secondary steering" effect, the substantial change of the power output for wind turbine running in the combined wake is much different from the conventional model prediction. This again supports the notion that when considering an array of more than two turbines operating in yawed conditions, the effect of vortex interactions must be taken into account.

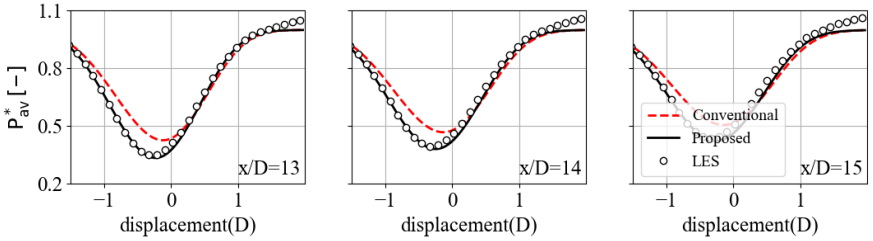

Figure 19. Power production of a hypothetical turbine behind the second turbine when the front turbine is yawed 20°: LES data (open circle), new proposed model (black solid line), and conventional analytical model (red dashed line).

4.2.3 Test case 3(two aligned wind turbines with the front one being yawed 30°)

In here, the contour plot of turbine wake in the third case are presented, which is a two-turbine scenario where the front turbine is yawed by 30°. As shown in Figure 20, for the wake flow downstream of the second turbine, continuous wake deflection is observed in SOWFA case, which is in line with previous analysis. Additionally, the prediction of the new model is found to be in good agreement with the LES results, it can well capture the steered wake in the superposed area.

However, in the conventional analytical model, since the influence of the persistent transverse velocity induced by the front yawed turbine is not considered, the prediction result greatly deviates from the reference case.

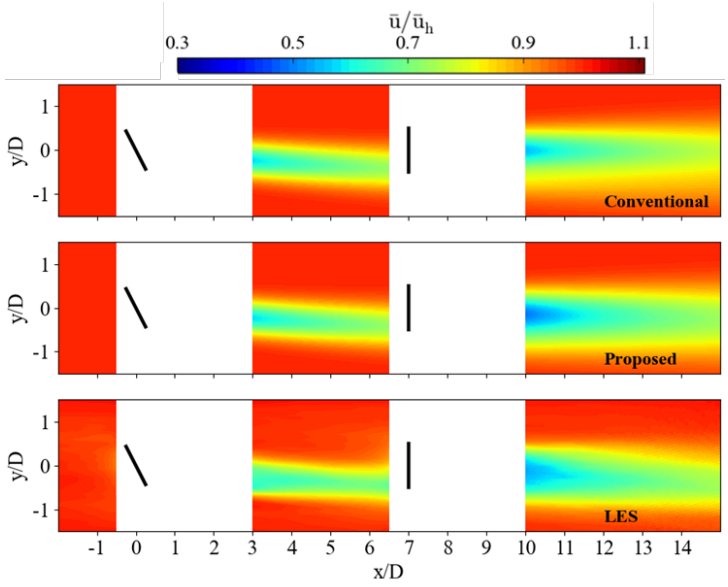

Figure 20. Contours of the normalized streamwise velocity in the horizontal hub-height plane for two aligned wind turbines when the front turbine is yawed 30°: Conventional analytical model(top), new proposed model (middle) and the large-eddy simulations (bottom).

Figure 21 presents the detailed lateral distribution of the velocity deficit at different downwind locations. As seen, the new proposed model agrees well with the LES data, showing the ability to capture the distribution characteristics of the streamwise wake . While for the conventional model, it fails to predict the wake deflection in the superposed area, and further, quite different from the reference wind field. To be specific, the velocity deficit in the lower half of the combined wake predicted by the conventional model is seriously under-estimated while the upper part is slightly over-estimated.

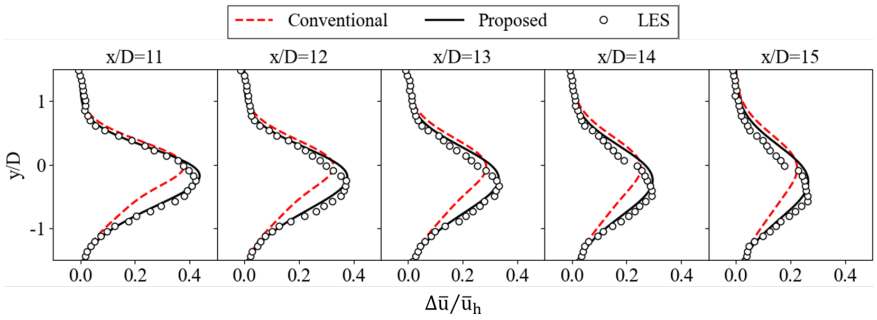

Figure 21. Lateral profiles of the normalized streamwise velocity deficit in the wakes at different downwind locations behind the second turbine when the front turbine is yawed 30°: LES data (open circle), new proposed model (black solid line), and conventional analytical model (red dashed line).

As evident in Figure 22, the regression analysis for Test Case 3 almost reproduces the results of Test Case 2, with the difference that, for the newly proposed model, the regression line is no longer so close to perfection; while for the conventional model, the deviation of the slope and intercept of the regression line from their ideal values becomes smaller. This outcome can be explained as follows: Different to the almost thoroughly underestimated velocity deficit in Test case 2, in Test Case 3 considered here, although the streamwise velocity deficit predicted by the conventional model is also lower than the LES data in the wake steering direction, it is slightly overestimated in another half part of the combined wake. It is the uneven distribution that leads to a relatively higher slope and a

lower intercept for the conventional model. Another striking observation in Figure 22 is the determination coefficient for the conventional model, whose value is the lowest among all the test cases of the two-turbine array, indicating a poor correlation between the model prediction and the reference case, and it also further highlights the necessity to develop new analytical models.

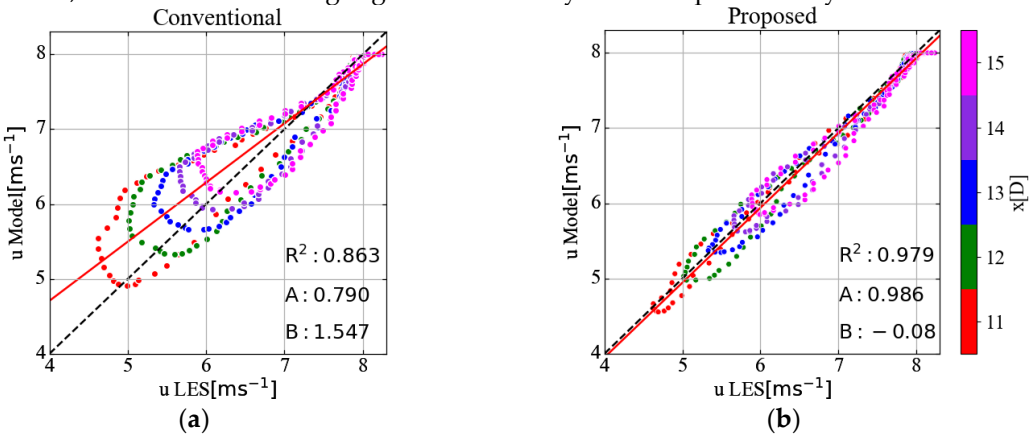

Figure 22. Scatter plot and corresponding regression line of the streamwise wake velocity as predicted using (a) the conventional analytical model and (b) the new proposed model, in relation to the reference wind field calculated with large-eddy simulations (LESs).

Figure 23 displays the power output for virtual wind turbines located in the superposed wake area, it can be observed that, the new analytical wind farm model provides a better prediction compared to the conventional one, but its result is less accurate on the right side, which may be related to the follow factors: For the single wake model adopted in the present work, the lateral velocity profile at hub height is assumed to have a symmetric Gaussian shape in the far wake. However, as indicated by previous experimental results [21], the wake profiles are slightly skewed by the strong transverse velocity distribution, especially for larger yaw angles. Furthermore, the partial-wake conditions experienced by the second wind turbine may be another contributor, it can give rise to an uneven wake recovery rate between the two sides of the wake. Consequently, in the right part of the power deficit "profile" in Figure 23, the new model shows a little deviation from the reference.

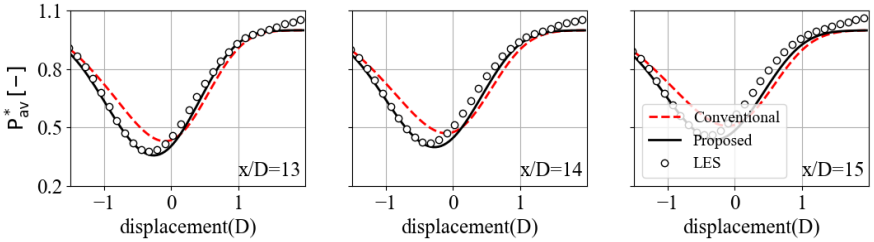

Figure 23. Power production of a hypothetical turbine behind the second turbine when the front turbine is yawed 30°: LES data (open circle), new proposed model (black solid line), and conventional analytical model (red dashed line).

4.2.4 Test case 4(three aligned wind turbines with the front one being yawed 20°)

In order to further investigate the "secondary wake steering" effect on wake evolution and evaluate the performance of analytical wake models, a three-turbine array simulation is performed, where the first wind turbine is yawed 20° and the other two turbines are maintained non-yawed. As apparent in Figures 24 and 25, the new proposed model is shown to be able to accurately predict deflections up to the third turbine's wake, consistent with the LES data. However, the conventional model based on sum of squares superposition method cannot capture such wake behavior. On the

one hand, this result indicates that the transverse velocity in upstream yawed turbine wakes, induced by the CPV, can persist past downwind turbines, even throughout the whole wind farm. Therefore, it is necessary to take its effects into wake model development and wake-redirection control design. On the other hand, the newly proposed model demonstrates its improvements in predicting for more than two turbines in a row under yawed conditions, addresses the concern about its universality, and also lays a foundation for its further application in the real-world engineering scenarios.

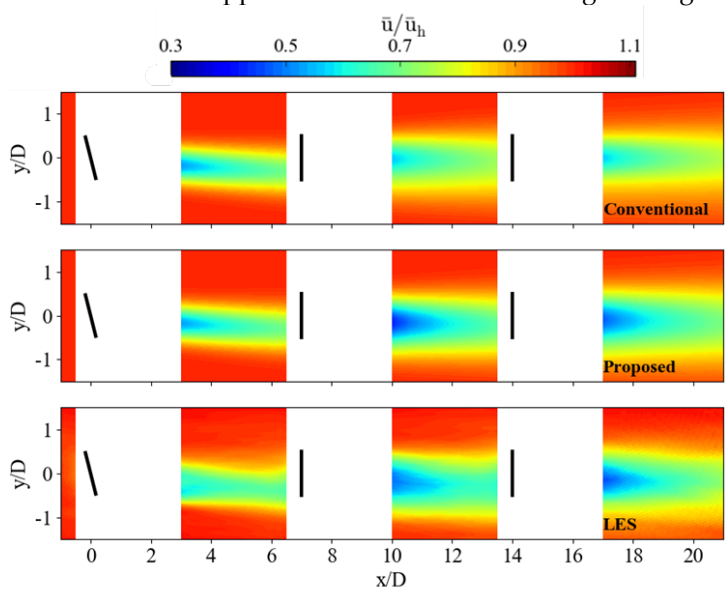

Figure 24. Contours of the normalized streamwise velocity in the horizontal hub-height plane for three aligned wind turbines when the front turbine is yawed 20°: Conventional analytical model(top), new proposed model (middle) and the large-eddy simulations (bottom).

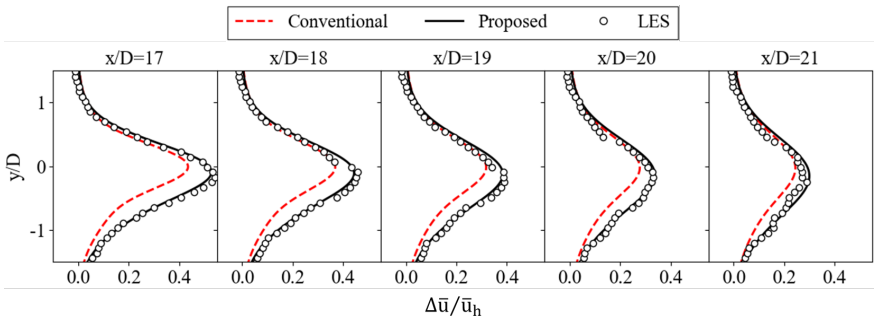

Figure 25. Lateral profiles of the normalized streamwise velocity deficit in the wakes at different downwind locations behind the third turbine when the front turbine is yawed 20°: LES data (open circle), new proposed model (black solid line), and conventional analytical model (red dashed line).

4.3. power output comparison

In this section, for assessing the predictive performance of analytical models on power output, simulations on another several two-turbine arrays are carried out. Panel (a) in Figure 26 shows the schematic diagram of yaw angle combinations, in which, the front wind turbine is always yawed 20°, while the second turbine is operating with different yaw misalignments: 15°(top row), 0°(middle row) and -15°(bottom row). With the same numerical settings of the test cases in Section 4.2, for the two-turbine array considered here, the inlet wind speed is 8 m/s and streamwise turbulence intensity at hub height is around 5.6% , and the separation between turbines is fixed at 7 times rotor diameter in the streamwise direction. Note that since the second wind turbine runs in a single yawed wake instead of a combined wake, the "secondary wake steering" effect has no impact on its power generation. In other words, the new proposed model for these cases is equivalent to only the "added yaw angle" effect addressed in Section 2.3.

Figure 26(b) shows the relative power gains for the second wind turbine in each yaw angle distribution relative to a baseline case of all turbines aligned. As apparent in the plot, in the conventional model predictions, the positive or negative yaw of the second turbine seems to have little effect on its power production. However, from the LES data, this is not the case. In particular, when the second turbine yaws towards the same direction as the first one, its power output is less than that when they yaw in opposite directions. This can be explained by the "added yaw angle". According to Equations (19) and (20), when the yaw direction of the two turbines is the same, the real yaw angle of the downstream wind turbine is greater than its set value, causing a decrease in its power generation, and vice versa. For the newly proposed model, since the effect of the "added yaw angle" is considered, it can well capture the asymmetric power distribution of the second turbine.

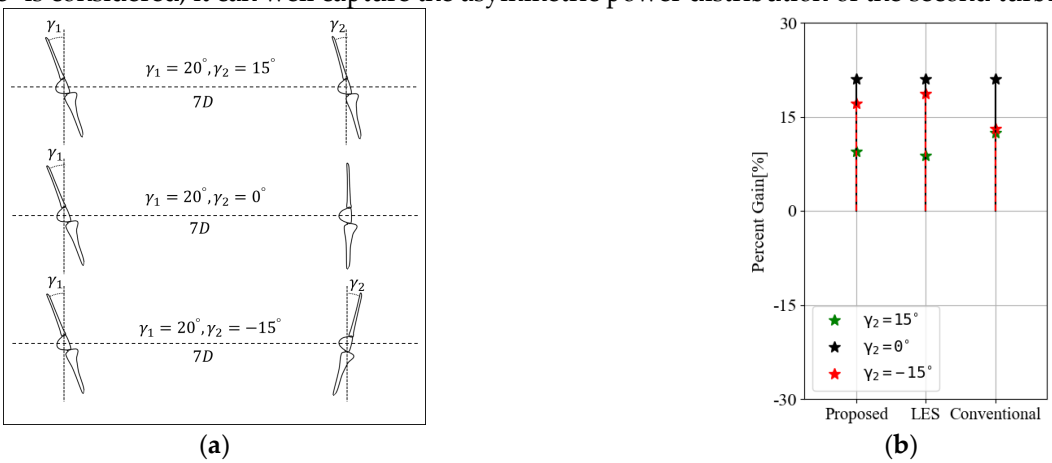

Figure 26. (a) Schematic diagram of the yaw angle distributions for two-turbine cases where the front turbine is yawed 20° and the second turbine is yawed 15° (top row), 0° (middle row), and -15° (bottom row). (b)Percent change of power production for the second turbine in each yaw angle distribution.

5. Conclusions

Recent studies have emphasized the importance of counter-rotating vortices in wake steering, these large-scale structures not only deform the wake of a yawed wind turbine, but also can make the wake trajectory of a non-yawed downwind turbine deviates from its rotor centerline, called “secondary wake steering” phenomenon. Due to these vortices can propagate a long distance, and thus, impact the wake steering performance of larger turbine arrays, it is necessary to include the effects of counter-rotating vortices in analytical wake model development and wind farm controller design. However, in the common analytical models for active yaw control, only the streamwise velocity from each individual wind turbine is calculated, without considering the transverse velocity induced by the vortex structures, this omission may lead to errors in model predictions. In order to compensate for it, a new analytical wind farm model is proposed, in which, a physical-based momentum-conserving wake superposition method [37] is adopted to model the interaction of multiple wakes; and in the application, not only the streamwise velocity is combined, but also the transverse velocity, which makes it possible to reproduce the secondary wake steering effect crucial to active yaw control. What's more, an "added yaw angle" is defined for a downwind turbine operating in upstream yawed turbine wakes, to reflect the change in local wind direction it perceives. Then, the total yaw angle including the defined "added yaw angle", instead of the set value of the yaw angle, is used as an input parameter for the single wake model derived by Wei and Wan[32] to calculate the individual wake.

For validation purposes, lots of numerical simulations are conducted using the SOWFA tool, and the obtained LES wind field is used as a reference to assess the analytical model performance. Detailed comparisons show that, the newly proposed model agrees well with LES results and outperforms the representative conventional analytical model in almost all test cases. In particular, the new model gives an accurate prediction on the wake velocity distribution in the superposed area, and can successfully reproduce the “secondary wake steering” phenomenon. By contrast, the

conventional model does not perform as such well, it tends to underestimate the total velocity deficit, and more importantly, the prediction results not support the aforementioned "secondary wake steering". The departure is largely because the sum of squares operation adopted to combine the wakes is an empirical formula without solid physical foundation, and no effects of the vortex interactions is considered. What's more, since the "added yaw angle" effect caused by the upstream transverse velocity is taken into account in the new model, it shows an ability to accurately predict the power gain of wake-affected downstream wind turbines.

In future studies, we will further evaluate the performance of the newly proposed analytical model in predicting deep turbine array (i.e., cases with several rows of wind turbines). Moreover, due to the merits of low computational cost and high accuracy, the new model will be used as a tool to explore the potential of active yaw control in wind farm power optimization.

Author Contributions: The paper was a collaborative effort among the authors. Dezhi Wei performed the modeling, designed the structure, and wrote the paper. Decheng Wan supervised the related work and polished the language of the paper.

Acknowledgments: This work was supported by National Natural Science Foundation of China (Grant No. 52131102, 51879159), National Key Research and Development Program of China (2019YFB1704200 and 2019YFC0312400), to which the authors are most grateful.

Conflicts of Interest: The authors declare no conflict of interest.

References

1. Gaumond, M.; Réthoré, P.E.; Ott, S.; Peña, A.; Bechmann, A.; Hansen, K.S. Evaluation of the wind direction uncertainty and its impact on wake modeling at the Horns Rev offshore wind farm. *Wind Energy* **2014**, *17*, 1169–1178.
2. Adaramola M.S.; Krogstad P.Å. Experimental investigation of wake effects on wind turbine performance. *Renew. Energy* **2011**, *36*, 2078–2086.
3. Dilip, D.; Porté-Agel, F. Wind turbine wake mitigation through blade pitch offset. *Energies* **2017**, 10, 757.
4. Lee, J.; Son, E.; Hwang, B.; Lee, S. Blade pitch angle control for aerodynamic performance optimization of a wind farm. *Renew. Energy* **2013**, *54*,124-130.
5. Fleming, P.A.; Gebraad, P.M.O.; Lee, S.; van Wingerden, J.W.; Johnson, K.; Churchfield, M.; Michalakes, J.; Spalart, P.; Moriarty, P. Evaluating techniques for redirecting turbine wakes using SOWFA. *Renew. Energy* **2014**, *70*, 211–218.
6. Bartl, J. M. S.; Muhle,F. V.; Sætran, L. R. Wind tunnel study on power output and yaw moments for two yaw-controlled model wind turbines. *Wind Energ. Sci.* **2018**, *3*, 489.
7. Campo, V.; Ragni, D.; Micallef, D.; Diez, F.J.; Simão-Ferreira, C.J. Estimation of loads on a horizontal axis wind turbine operating in yawed flow conditions. *Wind Energy* **2015**, 18(11), 1875-1891.
8. Bastankhah, M.; Porté-Agel, F. A wind-tunnel investigation of wind-turbine wakes in yawed conditions. *J. Phys. Conf. Ser.* **2015**, *625*, 012014.
9. Zong H, Porté-Agel, F. Experimental investigation and analytical modelling of active yaw control for wind farm power optimization. *Renew. Energy* **2021**, 170, 1228–1244.
10. Howland MF, Lele SK, Dabiri JO. Wind farm power optimization through wake steering. *Proc Natl Acad Sci* **2019**, 116(29), 14495-14500.
11. Lee, H.; Lee, D. Wake impact on aerodynamic characteristics of horizontal axis wind turbine under yawed flow conditions. *Renew. Energy* **2019**,136, 383-392.
12. van Dijk, M.; van Wingerden, J.W., Ashuri, T., Li, Y. Wind farm multi-objective wake redirection for optimizing power production and loads. *Energy* **2017**, 121, 561–569.
13. Bartl, Jan.; Mühle, F.; Sætran, L. Wind tunnel study on power output and yaw moments for two yaw-controlled model wind turbines. *Wind Energ. Sci.* **2018**, 3, 489–502.
14. Krogstad, P.; Adaramola, M.S. Performance and near wake measurements of a model horizontal axis wind turbine. *Wind Energy* **2012**, 15, 743–756.
15. Ozbay, A.; Tian, W.; Yang, Z.; Hu, H. Interference of wind turbines with different yaw angles of the upstream wind turbine. In Proceedings of the 42nd AIAA Fluid Dynamics Conference and Exhibit, New Orleans, LA, USA, 25-28 June 2012; p. 2719.

16. Bastankhah, M.; Porte-Agel, F. Wind tunnel study of the wind turbine interaction with a boundary-layer flow: Upwind region, turbine performance, and wake region. *Phys. Fluids* **2017**, 29, 065105.
17. Jiménez, Á.; Crespo, A.; Migoya, E. Application of a LES technique to characterize the wake deflection of a wind turbine in yaw. *Wind Energy* **2010**, *13*, 559–572.
18. Bartl, J.; Muhle, F.; Schottler, J.; Sætran, L.; Peinke, J.; Adaramola, M.; et al. Wind tunnel experiments on wind turbine wakes in yaw: Effects of inflow turbulence and shear. *Wind Energ. Sci.* **2018**, 3, 329–343.
19. Vollmer, L.; Steinfeld, G.; Heinemann, D.; Kühn, M. Estimating the wake deflection downstream of a wind turbine in different atmospheric stabilities: An LES study. *Wind Energ. Sci.* **2016**, *1*, 129–141.
20. Howland, M.F.; Bossuyt, J.; Martínez-Tossas, L.A.; Meyers, J.; Meneveau, C. Wake structure in actuator disk models of wind turbines in yaw under uniform inflow conditions. *J. Renew. Sustain. Ener.* **2016**, *8*, 043301.
21. Bastankhah, M.; Porté-Agel, F. Experimental and theoretical study of wind turbine wakes in yawed conditions. *J. Fluid Mech.* **2016**, *806*, 506–541.
22. Fleming, P.; Annoni, J.; Churchfield, M.; Martinez-Tossas, L.A.; Gruchalla, K.; Lawson, M.; et al. A simulation study demonstrating the importance of large-scale trailing vortices in wake steering. *Wind Energ. Sci.* **2018**, *3*, 243–255.
23. Bay, C.; King, J.; Fleming, P.; Mudafort, R.; Martinez, L. *Unlocking the full potential of wake steering: implementation and assessment of a controls-oriented model*; Technical Report; National Renewable Energy Lab. (NREL): Golden, CO(United States), 2019.
24. Bastankhah, M.; Porté-Agel, F. Wind farm power optimization via yaw angle control: A wind tunnel study. *J. Renew. Sustain. Ener.* **2019**, *11*, 023301.
25. Gebraad, P., Teeuwisse, F., Wingerden, J., Fleming, P.A., Ruben, S., Marden, J., et al. Wind plant power optimization through yaw control using a parametric model for wake effects – a CFD simulation study. *Wind Energy* **2016**, *19*, 95–114.
26. Jensen, N. *A note on wind turbine interaction*; Technical report; Ris-M-2411 Risø National Laboratory: Roskilde, Denmark, 1983.
27. Lin M.; Porté-Agel, F. Large-Eddy Simulation of yawed wind-turbine wakes: comparisons with wind tunnel measurements and analytical wake models. *Energies* **2019**, *12*, 4574.
28. Xie, S.; Archer, C. Self-similarity and turbulence characteristics of wind turbine wakes via large-eddy simulation. *Wind Energy* **2015**, *18*, 1815-1838.
29. Chamorro, L.; Porté-Agel, F. A wind-tunnel investigation of wind-turbine wakes: Boundary-layer turbulence effects. *Bound.-Layer Meteorol.* **2009**, *132*, 129–149.
30. Dou B, Guala M, Lei L, Zeng P. Wake model for horizontal-axis wind and hydrokinetic turbines in yawed conditions. *Appl. Energ.* **2019**, 242, 1383-1395.
31. Qian, G.W.; Ishihara, T. A new analytical wake model for yawed wind turbines. *Energies* **2018**, 11, 665.
32. Wei, D.Z, Wang, N.N, Wan, D.C. Modeling yawed wind turbine wakes: Extension of a Gaussian-based wake model. *Energies* **2021**, 14(15), 4494.
33. Katic, I.; Højstrup, J.; Jensen, N.O. A simple model for cluster efficiency. In Proceedings of the European Wind Energy Association Conference & Exhibition, Rome, Italy, 7–9 October 1986; pp. 407–410.
34. Shao, Z.Z.; Wu, Y.; Li, L.; Han, S.; Liu, Y.Q. Multiple wind turbine wakes modeling considering the faster wake recovery in overlapped wakes. *Energies* **2019**, *12*, 680.
35. Crespo, A., Hernández, J., Frandsen, S. Survey of modelling methods for wind turbine wakes and wind farms. *Wind Energy* **1999**, *2*, 1–24.
36. Martínez-Tossas, L.A.; Annoni, J.; Fleming, P.A.; Churchfield, M.J. The aerodynamics of the curled wake: A simplified model in view of flow control. *Wind Energ. Sci.* **2019**, *4*, 127–138.
37. Zong, H.H.; Porté-Agel, F. A momentum-conserving wake superposition method for wind farm power prediction. *J. Fluid Mech.* **2020**, *889*, A8.
38. Coleman, R.P.; Feingold, A.M. *Evaluation of the Induced-Velocity Field of an Idealized Helicoptor Rotor*; Wartime Report; UNT: Denton, TX, USA, 1945; p. 28.
39. Dou, B.; Qu, T.; Lei, L.; Zeng. P. Optimization of wind turbine yaw angles in a wind farm using a three-dimensional yawed wake model. *Energy* **2020**, 118415.
40. Kuo, J.; Pan, K.; Li, N.; Shen, H. Wind farm yaw optimization via random search algorithm. *Energies* **2020**, 13, 865.
41. Porté-Agel, F.; Wu, Y.T.; Chen, C.H. A numerical study of the effects of wind direction on turbine wakes and power losses in a large wind farm. *Energies* **2013**, *6*, 5297–5313

42. Abkar, M.; Porté-Agel, F. Mean and turbulent kinetic energy budgets inside and above very large wind farms under conventionally-neutral condition. *Renew. Energy* **2014**, *70*, 142–152.
43. Bastankhah, M.; Porté-Agel, F. A new analytical model for wind-turbine wakes. *Renew. Energy* **2014**, *70*, 116–123.
44. Niayifar, A.; Porté-Agel, F. Analytical modeling of wind farms: A new approach for power prediction. *Energies* **2016**, *9*, 741.
45. Thomas. J.; Annoni, J.; Fleming, P.; Ning, A. *Comparison of wind farm layout optimization results using a simple wake model and gradient-based optimization to large eddy simulations*; Technical Report; National Renewable Energy Lab. (NREL): Golden, CO(United States), 2019.
46. Quarton, D.; Ainslie, J. Turbulence in wind turbine wakes. *Wind Energy* **1990**, *14*, 15–23.
47. Frandsen, S.; Chacen, L.; Crespo, A.; *Measurements on and modeling of offshore wind farms*; Technical Report; Riso National Laboratory: Roskilde, Denmark, 1996.
48. Frandsen, S.; Thogersen, M.L. Integrated fatigue loading for wind turbines in wind farms by combining ambient turbulence and wakes. *Wind Energy* **1999**, *23*, 327–340.
49. Kirchner-Bossi, N.; Porté-Agel, F. Realistic wind farm layout optimization through genetic algorithms using a Gaussian wake model. *Energies* **2018**, 11, 3268.
50. Turner, S.; Romero, D.; Zhang, P.; Amon, C.; Chan, T. A new mathematical programming approach to optimize wind farm layouts. *Renew. Energy* **2014**, 63, 674–680.
51. Jonkman, J.; Butterfield, S.; Musial, W.; Scott, G. *Definition of a 5-MW reference wind turbine for offshore system development*; Technical Report; National Renewable Energy Lab.(NREL): Golden, CO, USA, 2009.
52. Jonkman, J.; Buhl M. *FAST user's guide*; Technical Report; National Renewable Energy Lab.(NREL): Golden, CO, USA, 2005.
53. Annoni. J.; Fleming, P.; Scholbrock, A.; Roadman, J.; Dana, S.; Adcock, C.; et al. Analysis of control-oriented wake modeling tools using lidar field results. *Wind Energ. Sci.* **2018**, 3, 819–831.
54. Burton, T.; Sharpe, D.; Jenkins, N.; Bossanyi, E. *Wind Energy Handbook*; John Wiley & Sons Ltd.: Chichester, UK, 2001; pp. 35–37. ISBN 0-471-48997-2.
55. Krogstad, P.A.; Adaramola, M.S. Performance and near wake measurements of a model horizontal axis wind turbine. *Wind Energy* **2012**, *15*, 743–756.
56. Pedersen, T. On wind turbine power performance measurements at inclined airflow. *Wind Energy* **2004**, *7*,163-176.
57. Dahlberg, J.; Montgomerie, B. *Research program of the utgrunden demonstration offshore wind farm*; Technical report; Swedish Defense Research Agency: Kista, Sweden, 2005.
58. Sørensen, J.N.; Shen, W.Z. Numerical modeling of wind turbine wakes, *J. Fluids Eng.* **2002**, *124*, 393–399.
59. Churchfield, M.J.; Lee, S.; Michalakes, J.; Moriarty, P.J. A numerical study of the effects of atmospheric and wake turbine dynamics. *J. Turbul.* **2012,** *13*, N14.

Nomenclature

Variables

x	downstream position from the wind turbine [m]	U_0	incoming wind velocity of the wind farm [m/s]
y	spanwise position from the turbine rotor center [m]	U_w	total streamwise velocity for the combined wake [m/s]
z	vertical position [m]	U_s	total streamwise velocity deficit for the combined wake [m/s]
D	diameter of wind turbine [m]	U_c	mean convection velocity for the combined wake [m/s]
z_h	turbine hub height [m]	V	total transverse velocity for the combined wake [m/s]
		γ_{set}	setting value of the yaw angle [°]

δ	wake center deflection [m]	γ_{added}	added yaw angle [°]
C_T	thrust coefficient	γ_{total}	total yaw angle [°]
C_{T0}	thrust coefficient at zero yaw	U_{equ}	equivalent resultant velocity acting at the rotor plane [m/s]
P	power output	I	turbulence intensity
P_0	power output at zero yaw	I_0	ambient turbulence intensity
k^*	wake width growth rate	I_+	added turbulence intensity
γ	yaw angle [°]	***Abbreviations***	
u_0	local wind speed perceived by the wind turbine [m/s]	CPV	a counter-rotating vortex pair
u_w	individual streamwise velocity [m/s]	2D	two-dimensional
u_s	individual streamwise velocity deficit [m/s]	3D	three-dimensional
u_c	mean convection velocity for the individual wake [m/s]	SS	sum-of-squares superposition method
v	individual transverse velocity [m/s]	MC	momentum conserving wake superposition method